

Supporting Information: Tailored Interfaces for Self-Patterning Organic Thin-Film Transistors

By: Jeremy W. Ward, Marsha A. Loth, R. Joseph Kline, Mariona Coll, Carmen Ocal, John E. Anthony, and Oana D. Jurchescu

PM-IRRAS Study of Fluorinated Self-assembled Monolayers (SAMs)

Fluorinated monolayers, 2-MFBT, 3-MFBT, 4-MFBT and PFBT, self-assembled on Au substrates were investigated by PM-IRRAS. Neat spectra of the four different molecules were also collected within 2 minutes of 2 μl deposition of molecules on a clean Au and Si substrate. Fig. SI 1 shows the IR spectra of the four SAMs and neat fluorinated molecules (a) 2-MFBT, (b) 3-MFBT, (c) 4-MFBT and (d) PFBT. In the four neat spectra 3 different groups of vibrations can be identified. The benzene ring compounds commonly exhibit several bands in the region 1600-1400 cm^{-1} attributed to C-C aromatic stretching modes.¹ Another group of vibrational bands appear in the range of 1300-1000 cm^{-1} and are assigned to C-H bending and C-F stretching modes.^{1,2} Finally, out-of-plane bending vibrations are observed below 1000 cm^{-1} . SAMs spectra show a reduced number of vibrational bands compared to neat molecules as a consequence of the IR surface selection rule, i.e. IR band with transition dipole moment, TDM, oriented parallel to the metal surface are absent.³ Therefore, preferential observation of some vibrational modes denotes a degree of molecular order in the monolayer. The peaks observed at 1600-1500 cm^{-1} are attributed to modes with a TDM along the S-aromatic ring axis,⁴ thus, a molecular geometry lying 100% parallel to the substrate surface is ruled out for the 3-MFBT, 4-MFBT and PFBT.⁵ Interestingly, 2-MFBT SAMs show peak shift frequency compared to 2-MFBT neat spectra that is not observed in the other 3 SAMs. This is likely attributed to a higher degree of molecular tilting. IR studies on fluorinated benzenethiols are rather limited but differences in molecular arrangement for substituted benzenethiols on a metal surface have been also identified by other techniques.⁶ For example, STM imaging studies on *para* and *ortho*-substituted halo benzenes identify significant differences in molecular packing and ordering of these two molecules. Lower surface coverage and a more inclined arrangement have been identified for the *ortho*-substituted molecules attributed to complex combination of interaction energies (i.e. dipole-dipole, S-F, quadrupole).⁷ Preferential orientation close to tangential has been reported for *para*-halosubstituted benzene rings and PFBT, in agreement with our results.⁷⁻⁹ Out-of-plane vibrations (associated dipole moment perpendicular to the phenyl ring) are extremely useful for quantitative orientational analysis;¹⁰ however, in our SAMs samples they could not be unambiguously identified (900-700 cm^{-1}) because they appear near to the detector cutoff and this spectral region becomes unreliable. Consequently, in this work we keep orientational analysis qualitative.

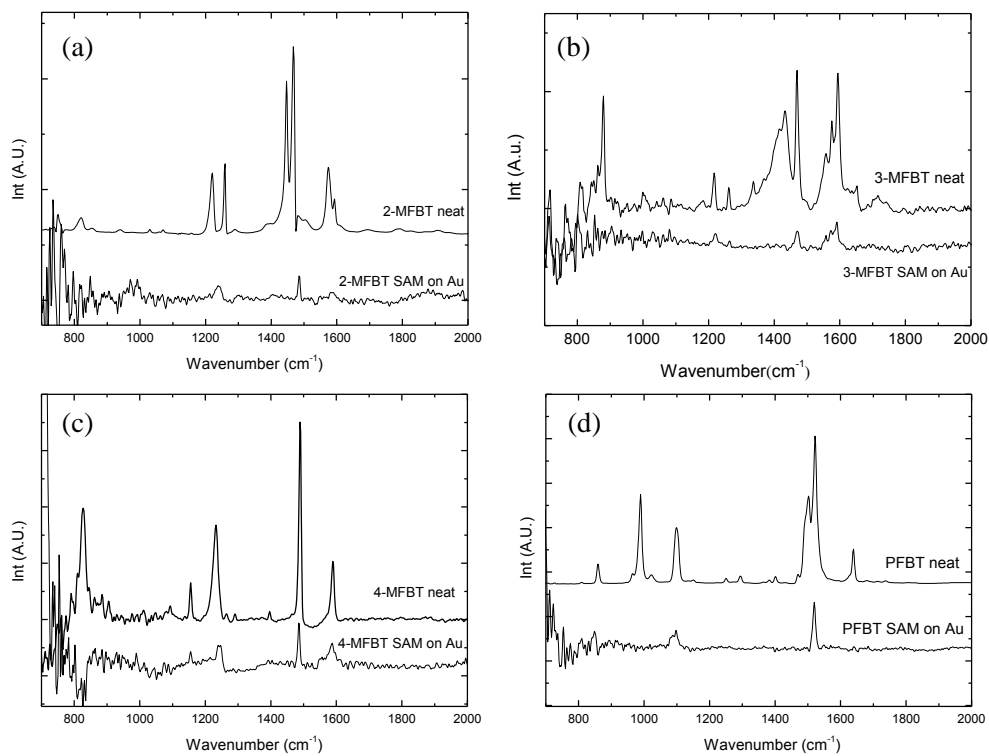


Fig. SI 1 PM-IRRAS of fluorinated SAMs and the corresponding neat spectra of (a) 2-MFBT, (b) 3-MFBT, (c) 4-MFBT and (d) PFBT.

Optical microscopy on Organic Semiconductor Thin-films

Optical micrographs taken on the FETs fabricated on bottom contacts chemically modified with the SAMs of interest are presented in Fig. SI 2. In Fig. SI 2a we present the case of untreated contacts, for comparison. This film consists of very fine grains and only a few distinguishable features. Fig. SI 2b-c, corresponding to the 2-MFBT and 3-MFBT, respectively, show a gradual increase in the grain size. Note that in all these cases the morphology of the film on the contact region is comparable to that observed on the oxide region of the FET. On the contrary, the devices presented in Fig. SI 2d-e, fabricated on contacts chemically tailored with 4-MFBT and PFBT, respectively, exhibit very different crystal habits, consisting of large grains on the contacts, protruding into transistor channel, and fine grains in the middle of the channel. Fig. SI 2f is a schematic representation of the differential microstructure present on the source-drain contact regions and the oxide regions.

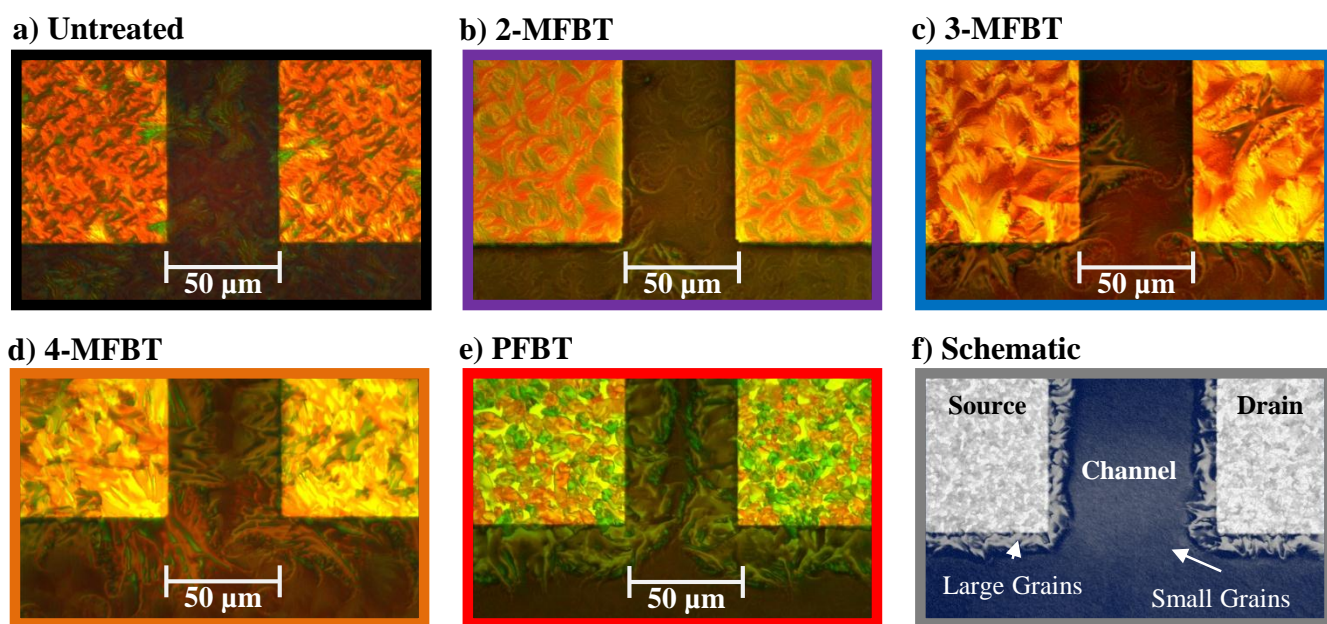


Fig. SI 2 Polarized optical micrographs showing diF-TES ADT thin-film characteristics on Untreated contacts (a), 2-MFBT (b), 3-MFBT (c), 4-MFBT(d), and PFBT (f) treated contacts. The OFET schematic (f) identifies differential microstructure on the contacts and the dielectric in devices.

GIXD on Organic Semiconductor Thin-films

Full pole figures are created by combining a local specular scan around the Bragg angle of the (001) peak with a GIXD plot as described by Baker et al.¹¹ The GIXD data is corrected for the polarization and the fixed incidence angle. To calculate the orientation fractions, the integration of the pole figures must include the change in solid angle as a function of χ . For samples with isotropic in-plane orientation, the total population of crystals at a given azimuthal tilt goes up with $\sin \chi$ while the pole figure measures a constant solid angle.¹² As a result, the pole figures substantially under-represents the crystal population at large azimuthal tilts.

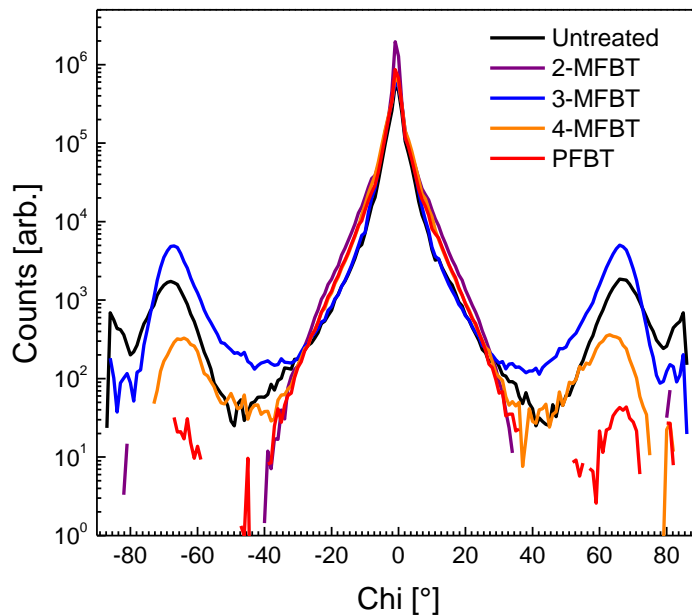


Fig. SI 3 GIXD full pole figure comparing relative intensities of a (001) peak for each treatment case.

Contact Resistance

For a set of devices having a fixed width, the total resistance is $R_{\text{on}} = \frac{\partial V_{\text{DS}}}{\partial I_{\text{D}}}$. We determine this in the linear regime of the device operation (i.e. $V_{\text{DS}} = -0.5$ V) and plot it as a function of channel length, L . Since $R_{\text{on}} = R_{\text{ch}}(L) + R_{\text{c}}$, where R_{c} is the contact resistance, we extrapolate the total resistance to $L=0$ to extract the contact resistance, R_{c} .¹³ Fig. SI 4 shows the width normalized contact resistance for each electrode surface as a function of gate voltage.

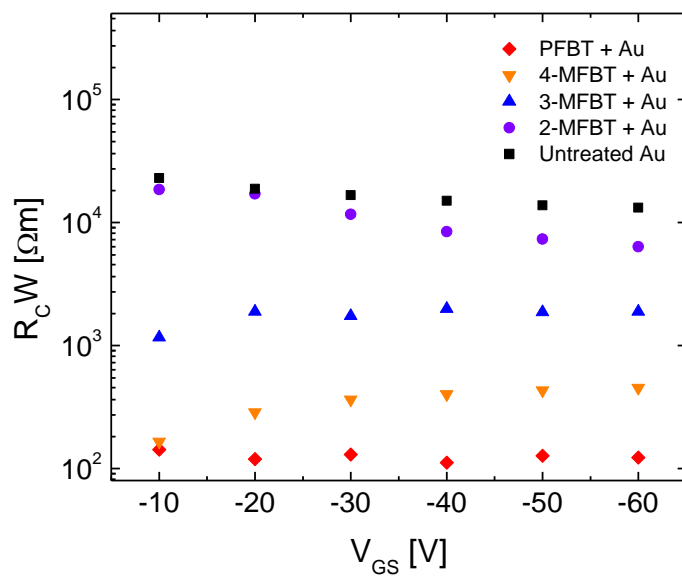


Fig. SI 4 Contact resistances as a function of gate voltage for bottom contact transistors of untreated Au contacts (black square), 2-MFBT (purple circle), 3-MFBT (blue triangle up), 4-MFBT (orange triangle down), and PFBT (red diamond) treated Au contacts.

Work Function Determination

The contact potential difference between the surface under test and probe surface ($V_{sample} - V_{probe}$), as measured by Kelvin probe, was used to determine the absolute work function using

$$\phi = -e(- (V_{sample} - V_{probe})) + \phi_{HOPG} \quad (1)$$

where 'e' is the electron charge, V_{sample} is the signal from sample, V_{probe} is the signal from the highly ordered pyrolytic graphite (HOPG) and $\phi_{HOPG} = 4.48\text{eV}$ is the work function of HOPG.¹⁴ All samples were stored in air for about 12 hours to allow for full solvent removal and film stabilization. PM-IRRAS measurements confirm that even longer air exposure does not produce degradation of the SAMs used in this study. Fig. SI 5 shows the measured work functions of each of the MFBT treated Au substrates. Uniformity between spots suggests a uniform SAM film on Au, while the consistency through time points to a stable electrode work function in the presence of the F-SAM treatments.

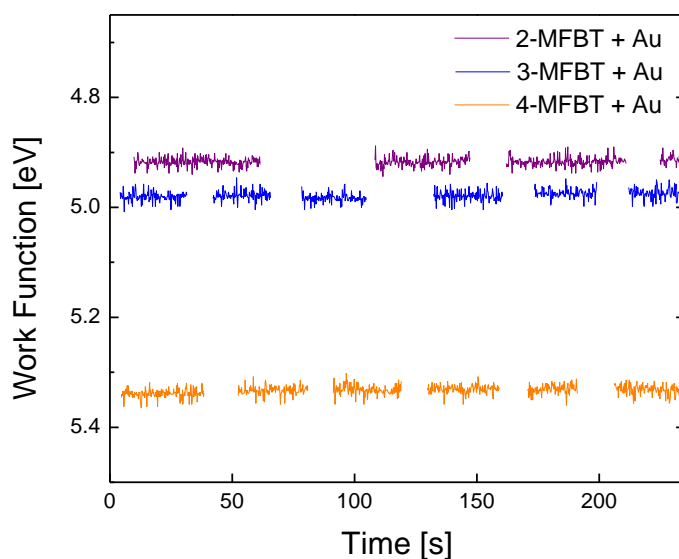
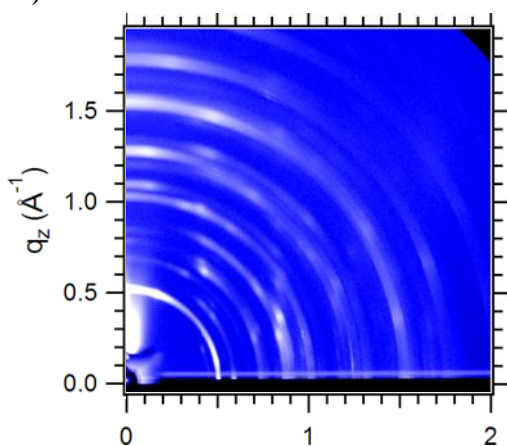


Fig. SI 5 The work function evolution throughout time as measured by Kelvin probe. The breaks in the signal represent the grounding of the detector during the movement to a different spot on the sample.

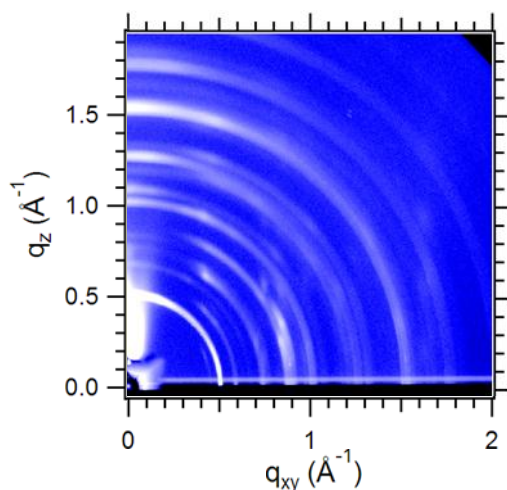
When does self-patterning not occur? The case of diF-TSBS ADT

To gain a metric into the F-F interaction strength between a SAM and organic semiconductor, we study the effect of surface treatments on the structure and electrical performance of an organic semiconductor with a chemical structure similar to diF-TES ADT, but a dramatically different molecular packing in the single crystal form. With difluoro-(tri-sec-butylsilyl ethynyl) anthradithiophene (diF-TSBS ADT – molecular structure in the inset of Fig. SI 5), the crystal packing motif is a sandwich herringbone and here the F-F interaction between the organic semiconductor and the F-SAM is not strong enough to induce a brick-layer packing that allows high mobility, like the case of diF-TES ADT.¹² This is supported by GIXD of diF-TSBS ADT films on both F-SAM treated and untreated substrates (Fig. SI 6a-b). Both cases exhibit the same sandwich-herringbone structure, in contrast with the co-facial packing observed in diF-TES ADT films. Additionally, the electrical properties of devices with PFBT treated and untreated contacts are identical (Fig. SI 6c).

a) PFBT Treated Contacts



b) Untreated Contacts



c) Electrical Properties

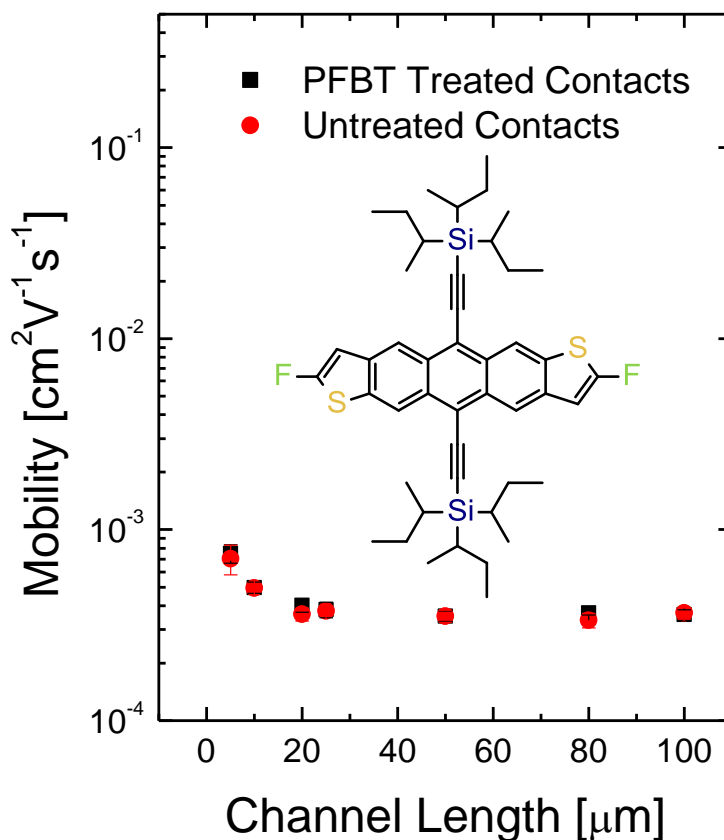


Fig. SI 6 GIXD on films of diF-TSBS ADT on a) PFBT treated Au and b) Untreated Au. c) Evolution of mobility with channel length for diF-TSBS ADT bottom contact devices fabricated on PFBT treated contacts (black square) and untreated (red circle) contacts.

References

- 1 A. M. Gardner, T. G. Wright, *The Journal of chemical physics*, 2011, **135**, 114305.
- 2 D. C. Smith, E. E. Ferguson, R. L. Hudson, J. R. Nielsen, *Journal of Chemical Physics*, 1953, **21**, 1475.
- 3 R. G. Greenler, *The Journal of Chemical Physics*, 1966, **44**, 310.
- 4 K. Rajalingam, L. Hallmann, T. Strunskus, A. Bashir, C. Woll, F. Tuzcek, *Physical Chemistry Chemical Physics*, 2010, **12**, 4390.
- 5 B. de Boer, H. Meng, D. F. Perepichka, J. Zheng, M. M. Frank, Y. J. Chabal, Z. Bao, *Langmuir*, 2003, **19**, 4272-4284.
- 6 C. A. Hacker, J. D. Batteas, J. C. Garno, M. Marquez, C. A. Richter, L. J. Richter, R. D. V. Zee, C. D. Zangmeister, *Langmuir*, 2004, **20**, 6195-6205.
- 7 P. Jiang, K. Deng, D. Fichou, S.-S. Xie, A. Nion, C. Wang, *Langmuir*, 2009, **25**, 5012-7.
- 8 H. Kang, Y. Kim, M. Hara, J. Noh, *Ultramicroscopy*, 2010, **110**, 666-9.
- 9 K. Wong, K.-Y. Kwon, B. V. Rao, A. Liu, L. Bartels, *Journal of the American Chemical Society*, 2004, **126**, 7762-3.
- 10 L.-J. Wan, M. Terashima, H. Noda, M. Osawa, *The Journal of Physical Chemistry B*, 2000, **104**, 3563-3569.
- 11 J. L. Baker, L. H. Jimison, S. Mannsfeld, S. Volkman, S. Yin, V. Subramanian, A. Salleo, a P. Alivisatos, M. F. Toney, *Langmuir*, 2010, **26**, 9146-51.
- 12 M. R. Hammond, R. J. Kline, A. a Herzing, L. J. Richter, D. S. Germack, H.-W. Ro, C. L. Soles, D. a Fischer, T. Xu, L. Yu, M. F. Toney, D. M. DeLongchamp, *ACS Nano*, 2011, **5**, 8248-57.
- 13 S. M. Baier, M. S. Shur, K. Lee, N. C. J. Cirillo, S. A. Hanka, *IEEE Transactions on Electron Devices*, 1985, **32**, 2824-2829.
- 14 W. N. Hansen, G. J. Hansen, *Surface Science*, 2001, **481**, 172-184.